

Photons from axial-vector radiative decay in a hadron gas

Kevin Haglin*

*National Superconducting Cyclotron Laboratory, Michigan State University
East Lansing, Michigan 48824-1321*

(May 6, 2019)

Abstract

Strange and non-strange axial-vector meson radiative decays contribute to photon production in hadron gas. One- and two-hadron radiative decay modes of $b_1(1235)$, $a_1(1260)$ and $K_1(1270)$ are studied. At 200 MeV temperature and for a narrow range in photon energies they contribute more to the net thermal photon production rate than $\pi\rho \rightarrow \pi\gamma$, $\pi\pi \rightarrow \rho\gamma$ or $\rho \rightarrow \pi\pi\gamma$. They provide significant contribution to the rate for photon energies as high as 1.5–2.0 GeV. For higher energies they are less important.

PACS numbers: 25.75.+r, 12.38.Mh, 13.75.Lb

I. INTRODUCTION

Photons are able to probe any or all stages of a relativistic heavy-ion collision [1] since their mean free paths are much larger than the transverse size of the hot and dense region and will therefore escape after production without rescattering. Massive photons, or dileptons, share this property. Therefore, photons and dileptons are thought to provide exciting means of probing even the central region cleanly [2–8]. Observation of quark-gluon plasma through the use of photons is contingent, among other things, on the production rate or ultimately the yield being distinguishable from hadron gas. Yet, current understanding is that hadron gas and quark-gluon plasma produce energetic photons nearly equally frequently at fixed temperature ≈ 200 MeV [9]. While studying low-mass dilepton spectra after integrating the rates over space-time history the same conclusion was reached: the two phases produced massive photons more or less equally [10]. If any important contribution has been ignored, e.g. strange particles or heavy mesons, it would be very useful to know about such things.

Within the hadron gas photon production will originate in many ways as there may be several hadronic species produced directly or perhaps pair-produced thermally since the temperatures can rise to extreme values and approach the critical value T_c , somewhere in the range 150–200 MeV, where crossover to the deconfined and chirally symmetric phase is presumed to be. Produced photons might be categorized according to their energy as follows. For E_γ below 0.5 GeV bremsstrahlung from charged particle scattering and decay will be important. Also, reactions in which a large mass hadron (compared to the combined mass of the initial hadrons) is in the final state such as $\pi\pi \rightarrow \rho\gamma$ are endothermic and tend to give large contributions at low photon energies. For higher energies direct decays give a substantial contribution as does the process $\pi\rho \rightarrow \pi\gamma$. It has recently been shown that inclusion of the a_1 resonance in $\pi\rho \rightarrow \pi\gamma$ scattering results in a large rate of photon production, larger than all others combined [11]. When interference effects are treated properly the effect of the a_1 is changed somewhat but remains important [12]. Vector meson decays are also important: the ω has a relatively large decay rate into a neutral pion and photon. Folding in a Bose-Einstein distribution for the ω results in a significant thermal production rate [9]. Kaon abundances are 2–3 times smaller than pion’s at temperatures near T_c , so they will frequently scatter with pions and with rhos. With the pions, $K^*(892)$ resonances can be formed and with the rhos, scattering through $K_1(1270)$ is probable. The $K\rho$ decay channel of $K_1(1270)$ is exceptional in that it is only 71 MeV/c center-of-mass momentum above threshold and therefore has a cross section (proportional to $1/p_{c.m.}^2$) which is relatively large. This resonance has recently been shown to affect kaon mean free paths in hot matter by tens of percents [13]. It is therefore interesting to study reactions involving the K_1 and their contributions to photon production.

The large family of non-strange and strange mesons will comprise the hot thermalized system. At temperatures near 100 MeV or so, the system will be populated mostly by pions since Boltzmann weightings strongly suppress the heavier ones. As the temperature rises to something near T_c , the situation can become different since the suppression is effectively weaker. Using zero chemical potentials in Boltzmann distributions at a temperature of 200 MeV, there are 2.9×10^{-1} π s, 1.5×10^{-1} ρ s and 1.3×10^{-1} K^* s per fm^3 , while there are 2.9×10^{-2} $K_1(1270)$ s and 2.6×10^{-2} $b_1(1235)$ s per fm^3 [13]. The latter is quite important because it decays predominantly into a $\pi\omega$ combination and has a full width of 155 ± 8 MeV. The

ω might be on shell in which case it just contributes to the equilibrium number of omegas. It might also be off shell and will subsequently decay (off shell) into $\pi^0\gamma$. The product of the density times overall decay seems sizeable, so folding in the dynamics, kinematics and thermally distributed phase space could result in a significant thermal production rate.

Theoretical framework for photon production rates through radiative decay from a thermalized system will be presented in the next section. Discussion of the model dependence of hadronic and electromagnetic transitions upon their specific interactions will also appear. They are modelled by effective Lagrangians describing both $AV\phi$ and $VV'\phi$ three-point vertices, where A is an axial-vector field, V and V' are vector fields and ϕ is a pseudoscalar field. Then in section III results are presented for one- and two-hadron radiative decays for a temperature 200 MeV. The channel $b_1 \rightarrow \pi\pi^0\gamma$ is found to be important, and so further dependence on temperature is studied. Section IV contains an estimate for the collisional broadening of ω in the above mentioned b_1 radiative decay. Modified photon production rates follow. Finally, section V contains concluding remarks and possible ramifications of these results.

II. THERMAL RADIATIVE DECAY

The rate for photon production from a thermalized system at temperature T whose size is small relative to the photon mean free path is proportional to the imaginary part of the retarded photon self-energy $\Pi_R^{\mu\nu}$ and a thermal weighting as [15–17]

$$E_\gamma \frac{dR}{d^3p_\gamma} = \frac{-2g^{\mu\nu}}{(2\pi)^3} \text{Im}\Pi_{\mu\nu}^R \frac{1}{e^{E_\gamma/T} - 1}. \quad (2.1)$$

For temperatures $100 < T < T_c$, the largest contributions to the self-energy will be one- and two-loop diagrams consisting of π s and ρ s. Near T_c , contributions from diagrams in which heavier non-strange and strange particles occupy the loops also become important. Figure 1a shows one-loop πa_1 and KK_1 contributions, and 1b shows a two-loop $\pi\omega$ contribution [with ω further splitting to $b_1\pi$]. If the imaginary part of any of these diagrams (obtained by cutting them) gives a calculated width in vacuum that is relatively sizeable, then even being less abundant than pions or rhos in the hot system, it is interesting to ask about their contributions to photon production. Cutting the diagram in Fig. 1a results in single-hadron radiative decays of either a_1 or K_1 axial-vectors. They are shown in Fig. 2a. The diagram in Fig. 1b is of two-loop order and therefore its cut diagram has four external lines. Kinematics allows two possibilities for the photon being in the final state. First, there could be $\pi b_1 \rightarrow \omega \rightarrow \pi^0\gamma$ scattering. Secondly, a two-pion radiative decay $b_1 \rightarrow \omega\pi \rightarrow \pi\pi^0\gamma$ can proceed. The production rate from the first process turns out to be rather unimportant as compared with the second. Its diagram is in Fig. 2b.

Elementary radiative hadron decays, $h_a \rightarrow \sum_b h_b + \gamma$, can proceed in two ways. One of the incoming or outgoing particles can emit a photon (bremsstrahlung) or secondly, the photon can be emitted directly. Direct emission reflects the internal structure and has vanishing phase space for vanishing photon energy. In a thermal calculation the decay rate is important but so too is the number density of the decaying hadron. Besides $\rho \rightarrow \pi\pi\gamma$, the many-hadron final states have been neglected since they were assumed small. But as will soon be seen, at least one is not. The thermal rate for radiative hadronic decay is

$$E_\gamma \frac{dR}{d^3p_\gamma} = \mathcal{N} \int \frac{d^3p_a}{(2\pi)^3 2E_a} f(E_a) |\mathcal{M}|^2 (2\pi)^4 \delta^4(p_a - p_1 - \dots - p_n - p_\gamma) \\ \times \left\{ \prod_{i=1}^n \frac{d^3p_i}{(2\pi)^3 2E_i} [1 \pm f(E_i)] \right\} \frac{1}{(2\pi)^{3/2}}. \quad (2.2)$$

where \mathcal{N} is the degeneracy and $f(E)$ is either a Bose-Einstein or Fermi-Dirac distribution depending on the species. Bose enhancement (Pauli suppression) is enforced by choosing the $+$ ($-$) sign in the square-bracketed term. Identifying the species of hadrons and their interaction with other hadrons into which they might decay, and specifying their interaction with the electromagnetic field completely defines the problem. What remains is to carry out the necessary four-vector algebra and phase space integration.

The model Lagrangians used are the following. First for the $AV\phi$ interaction [11]

$$L_{AV\phi} = g A^\mu ((p_V \cdot p_\phi) g_{\mu\nu} - p_{V\mu} p_{\phi\nu}) V^\nu \phi, \quad (2.3)$$

and then for the $VV'\phi$ vertex [18]

$$L_{VV'\phi} = g' \epsilon_{\mu\nu\alpha\beta} p_V^\mu V^\nu p_{V'}^\alpha V'^\beta \phi \quad (2.4)$$

where $\epsilon_{\mu\nu\alpha\beta}$ is the totally antisymmetric unit tensor. Modelling the interactions depicted by vertices in the diagrams of Figs. 2a and b this way, their individual decay widths are calculated to be

$$\Gamma_{\omega \rightarrow \pi^0 \gamma} = \frac{g_{\omega\pi^0\gamma}^2}{12\pi m_\omega^2} |\mathbf{p}| (p_{\pi^0} \cdot p_\gamma)^2 \quad (2.5)$$

$$\Gamma_{b_1 \rightarrow \pi\omega} = \frac{g_{b_1\pi\omega}^2}{24\pi m_{b_1}^2} |\mathbf{p}| \left(2(p_\pi \cdot p_\omega)^2 + m_\omega^2 (m_\pi^2 + \mathbf{p}^2) \right) \quad (2.6)$$

$$\Gamma_{a_1 \rightarrow \pi\rho} = \frac{g_{a_1\pi\rho}^2}{24\pi m_{a_1}^2} |\mathbf{p}| \left(2(p_\pi \cdot p_\rho)^2 + m_\rho^2 (m_\pi^2 + \mathbf{p}^2) \right) \quad (2.7)$$

and

$$\Gamma_{K_1 \rightarrow \rho K} = \frac{g_{K_1\rho K}^2}{24\pi m_{K_1}^2} |\mathbf{p}| \left(2(p_K \cdot p_\rho)^2 + m_\rho^2 (m_K^2 + \mathbf{p}^2) \right), \quad (2.8)$$

where \mathbf{p} is the center-of-mass momentum of the decay products. These determine the coupling constants to be $g_{\omega\pi^0\gamma} = 0.7$, $g_{b_1\pi\omega} = 10.3$, $g_{a_1\pi\rho} = 14.8$ and $g_{K_1\rho K} = 12.0 \text{ GeV}^{-1}$ in order that the partial decay widths are 0.7, 155, 400 and 37.8 MeV respectively, so they match results from the Review of Particle Properties [19].

An estimate for coupling the axial-vectors a_1 and K_1 to the photon field (and a pion or kaon respectively) is now needed. Decay of the b_1 into a pion and photon is not considered since it results in a small rate. Here is where a model is employed since no experimental information on these decays exist. By vector-meson dominance, the coupling for these are

$$g_{a_1\pi\gamma} = (e/f_\rho) g_{a_1\rho\pi} \\ g_{K_1K\gamma} = (e/f_\rho) g_{K_1\rho K} \quad (2.9)$$

where $f_\rho^2/4\pi = 2.9$ is the $\rho\pi\pi$ coupling. Numerically these coupling constants become $g_{a_1\gamma\pi} = 0.74 \text{ GeV}^{-1}$ and $g_{K_1\gamma K} = 0.60 \text{ GeV}^{-1}$. Using the calculated expressions

$$\Gamma_{a_1 \rightarrow \gamma\pi} = \frac{g_{a_1\gamma\pi}^2}{12\pi m_{a_1}^2} |\mathbf{p}| (p_\gamma \cdot p_\pi)^2 \quad (2.10)$$

$$\Gamma_{K_1 \rightarrow \gamma K} = \frac{g_{K_1\gamma K}^2}{12\pi m_{K_1}^2} |\mathbf{p}| (p_\gamma \cdot p_K)^2, \quad (2.11)$$

electromagnetic decay widths of $\Gamma_{a_1 \rightarrow \gamma\pi} = 1.4 \text{ MeV}$ and $\Gamma_{K_1 \rightarrow \gamma K} = 1.5 \text{ MeV}$ are obtained.

Matrix elements for photon production corresponding to the processes in Fig. 2a for a_1 and K_1 decay are

$$\mathcal{M} = g_{a_1\gamma\pi} \epsilon_{a_1}^\mu \left((p_\pi \cdot p_\gamma) g_{\mu\nu} - p_{\gamma\mu} p_{\pi\nu} \right) \epsilon_\gamma^\nu \quad (2.12)$$

and

$$\mathcal{M} = g_{K_1\gamma K} \epsilon_{K_1}^\mu \left((p_K \cdot p_\gamma) g_{\mu\nu} - p_{\gamma\mu} p_{K\nu} \right) \epsilon_\gamma^\nu, \quad (2.13)$$

where the ϵ s are polarization vectors for the respective (vector) fields. Each one depends therefore on a spin index which is not explicitly written. The two-pion radiative decay depicted in Fig. 2b has a matrix element of

$$\mathcal{M} = g_{b_1\pi\omega} g_{\omega\pi^0\gamma} \epsilon_{b_1}^\mu \left((p_\pi \cdot p_\omega) g_{\mu\nu} - p_{\omega\mu} p_{\pi\nu} \right) D^{\nu\alpha} \epsilon_{\beta\alpha\sigma\lambda} p_\omega^\beta p_\gamma^\sigma \epsilon_\gamma^\lambda \quad (2.14)$$

where the pion momenta refer to the pion emitted from the $b_1\omega\pi$ vertex in the diagram of Fig. 2b and the propagator for the ω in the same diagram is

$$D^{\nu\alpha}(l) = (g^{\nu\alpha} - l^\nu l^\alpha / m_\omega^2) \frac{1}{l^2 - m_\omega^2 - im_\omega \Gamma_\omega}. \quad (2.15)$$

The width is taken as the vacuum value of $\Gamma_\omega = 8.43 \text{ MeV}$, although modification due to the presence of matter will be discussed later. Squaring the matrix elements, contracting all the indices and summing over spin states is the first step. Using Eq. (2.2) the production rate reduces to an integral over one- and two-particle phase space respectively, for processes from Figs. 2a and b.

III. RESULTS

Thermal photon production rates at 200 MeV temperature for the processes $a_1 \rightarrow \pi\gamma$, $K_1 \rightarrow K\gamma$ and $b_1 \rightarrow \pi\pi^0\gamma$ are shown in Fig. 3. Results for $a_1 \rightarrow \pi\pi\gamma$ and $K_1 \rightarrow K\pi\gamma$ will not be discussed here since they result in smaller rates. Features common to these processes are that they turn over and approach zero for $E_\gamma \rightarrow 0$ simply due to vanishing phase space in this limit. Unlike processes such as $\rho \rightarrow \pi\pi\gamma$, these axial-vector *direct* decays cannot proceed without the photon present. They peak at slightly different photon energies due to the differences in the axial-vector and decay particle masses. Their slopes also reflect these differences: the $K\gamma$ shows the largest slope, then the $\pi\pi^0\gamma$ followed by the $\pi\gamma$ final state results. The most startling feature is the overall magnitude of the b_1 decay. For this

temperature its peak is seven times larger than the others. The reason for this is twofold. First is the relative abundance of b_1 , for which there are roughly half as many b_1 s as there are omegas per unit volume. This is larger than one would expect, but isospin degeneracy and the high temperature are responsible. Secondly, b_1 decays predominantly into a $\pi\omega$ combination, which subsequently decays into $\pi\pi^0\gamma$. Roughly speaking, the overall rate for this is

$$\frac{\Gamma_{b_1 \rightarrow \pi\omega} \Gamma_{\omega \rightarrow \pi^0\gamma}}{\Gamma_{\omega}^{\text{full}}} = 13.2 \text{ MeV}, \quad (3.1)$$

which is a factor 18 larger than simple $\omega \rightarrow \pi^0\gamma$ decay. Multiplying the density of b_1 mesons times the rate from Eq. (3.1) results in a factor 9 more than radiative ω decay. When comparing thermal photon production via $b_1 \rightarrow \pi\pi^0\gamma$ with the corresponding thermal production rate for $\omega \rightarrow \pi^0\gamma$ presented at $T = 200$ MeV in Ref. [9], this factor of 9 is consistent. Kinematics and Bose-Einstein distributions complicate matters as does the phase space integration, but the result can be understood with the above simple argument.

One-pion radiative decay of real omegas is not included within the b_1 decay—they really are separate contributions. Imagine b_1 being instead very massive. Thermal photon production via b_1 decay would approach zero in the infinite-mass limit simply due to vanishing equilibrium number density $\bar{n}_{b_1} \rightarrow 0$. Omega radiative decay, on the other hand, is not affected by such a change and ω decay must contribute. Summing both processes does not amount to double counting.

Radiative decay of b_1 turns out to be rather large (for a limited range in photon energy) due in part to the abundance. The natural question to ask therefore, is about its rise with increasing temperature; or alternatively, its fall with decreasing temperature. For this reason Fig. 4 is shown at three values of temperature 100, 150 and 200 MeV. Each result is superimposed on the rate of photon production from $\pi\rho \rightarrow \pi\gamma$ as calculated using an effective chiral Lagrangian including effects of the a_1 resonance coherently [12]. As the temperature drops, the photon energy for which the two processes are equal shifts downward. But the noteworthy feature of dominance of the two-pion radiative decay of b_1 for a narrow range of photons energies basically remains even at temperature 100 MeV.

IV. COLLISIONAL BROADENING OF OMEGA

The hadron-gas environment is quite different from free space, and one can therefore justifiably question the applicability of the matrix element of Eq. (2.14). In particular, the ω propagator is just taken to be the free space vector propagator which contains the vacuum width of 8.43 MeV and no shift in pole position. The vacuum width corresponds to a lifetime of 23 fm/c. Yet, the mean free path of an ω in this hot matter is at most a few fermis since it can scatter with pions to form a b_1 resonance [20], so it will likely rescatter before decaying. To account for this, a collisional broadened width is computed. Roughly it is $n\sigma v$, where n is the pion density, σ is the $\pi\omega$ cross section, and v is their relative velocity. If there are 0.3 pions per fm³, if the cross section is 1 fm² and the relative velocity $v/c = 0.5$, an extra *collisional* width of 30 MeV should be added to the vacuum width. Rather than use this crude estimate, the expression

$$\Gamma_{\omega}^{\text{coll}}(E_{\omega}) = \int ds \frac{d^3 p_{\pi}}{(2\pi)^3} f(E_{\pi}) \sigma_{\pi\omega}(s) v_{\text{rel}} \delta\left(s - (p_{\pi} + p_{\omega})^2\right) \quad (4.1)$$

is used, where

$$v_{\text{rel}} = \frac{\sqrt{(p_{\pi} \cdot p_{\omega})^2 - 4m_{\pi}^2 m_{\omega}^2}}{E_{\pi} E_{\omega}}. \quad (4.2)$$

A Breit-Wigner form for the cross section

$$\sigma_{\pi\omega}(\sqrt{s}) = \frac{\pi}{\mathbf{k}^2} \frac{\Gamma_{b_1 \rightarrow \pi\omega}^2}{(\sqrt{s} - m_{b_1})^2 + \Gamma_{b_1}^2/4} \quad (4.3)$$

is used with \mathbf{k} being the center-of-mass momentum and the full and partial widths taken to be 155 MeV. The collision rate (or width) is presented in Fig. 5 for 100, 150 and 200 MeV temperature. Energy dependence aside, it is indeed of order 30 MeV. It is now added to the vacuum width resulting in an energy-dependent full width of

$$\Gamma_{\omega}^{\text{full}}(E_{\omega}) = \Gamma_{\omega}^{\text{vac}} + \Gamma_{\omega}^{\text{coll}}(E_{\omega}). \quad (4.4)$$

The propagator of Eq. (2.15) is now modified by replacing the omega width by this energy-dependent full width $\Gamma_{\omega} \rightarrow \Gamma_{\omega}^{\text{full}}(E_{\omega})$. Integrating over the phase space for the initial and final hadrons as in Eq. (2.2) sums over contributions from all kinematically allowed squared four momentum for the omega. A broader total width in the (denominator of the) propagator will naturally reduce the rate for producing photons. In physical terms, the propagating omega from which radiation originates can scatter with the strongly interacting matter and is therefore no longer as free to decay radiatively. Modified rates are compared in Fig. 6 with those using the vacuum width. The reduction in photon production is more pronounced at larger temperatures as expected but for temperature 100–200 MeV, the modified rate is comparable to $\pi\rho \rightarrow \pi\gamma$ at its peak. However, it is no longer significantly larger than the other axial-vector decays considered here.

To more fully appreciate the relative importance of radiative decay Fig. 7 is shown. In it, the sum of a_1 , b_1 and K_1 decays is compared at $T = 200$ MeV with the dominant hadronic scattering contributions $\pi\rho \rightarrow \pi\gamma$ and $\pi\pi \rightarrow \rho\gamma$ as well as the decay $\rho \rightarrow \pi\pi\gamma$ taken from Ref. [12]. The b_1 results are those from Fig. 6 which include a collisional broadened width for the omega. Radiative decays contribute more than scattering for photon energies 0.4–0.75 GeV. Then for more energetic photons they are less important. If one is merely concerned with the overall order of magnitude of the photon energy spectrum, these are clearly not so important. At some level in more detailed analyses of the energy spectrum, these axial-vector radiative decays do become important.

V. CONCLUDING REMARKS

Mechanisms for photon production in hot hadronic matter are numerous. Most of them involve species whose abundances are too low or whose scattering rates or decay rates are too small to compete with pion and rho meson processes. There are some with abundances

and relevant rates that do in fact compete for limited range in photon energies. Namely, radiative decay of the heavier axial-vector mesons a_1 , b_1 and K_1 are relatively important. Contributions from $a_1 \rightarrow \pi\gamma$ and $K_1 \rightarrow K\gamma$ are comparable to $\omega \rightarrow \pi^0\gamma$ with similar photon energy dependence. Contribution of $b_1 \rightarrow \pi\pi^0\gamma$ is as large as $\pi\rho \rightarrow \pi\gamma$ near its peak which occurs at photon energy 0.5 GeV. However, for photon energies 0.4 GeV and less, other processes like $\pi\pi \rightarrow \rho\gamma$ and $\rho \rightarrow \pi\pi\gamma$ become dominant [9,12]. Other heavy mesons do not contribute as strongly as the three axial-vector radiative decays mentioned above. The $\pi\rho$ and $K\rho$ decay channels of a_1 and K_1 are very strong which result in rather large coupling constants. By vector-meson dominance, the electromagnetic-decay coupling constants are also relatively large. Similar remarks can be made about the b_1 , but in addition it is also exceptional since one of its most likely decay products is ω . The ω 's electromagnetic decay rate is rather large—a partial width of 0.7 MeV. Other non-strange and strange heavy mesons which decay to omega do so with much smaller rates and furthermore, will not be nearly so abundant at temperatures 100–200 MeV.

Thermalization is assumed for all hadronic species in this study. For pions and rho mesons this is quite reasonable but for heavier hadrons it is not so clear. It may well be that the axial-vectors considered here do not thermalize. Their average dynamics could be different resulting in different photon production. Modification due to such effects would be an interesting pursuit.

The method of collisional broadening included in Sec. IV is somewhat simplistic. One should really compute a finite temperature propagator and self-energy for the omega to two-loop order. The presence of matter modifies the width by modifying the imaginary part of the self-energy. It also modifies the pole position of the propagator, i.e. gives the omega an effective mass, by introducing a real part to the self-energy. Such a calculation would have appeal from the point of view of theory that the real and imaginary parts would be computed consistently. What has been done in the present work represents only a simple, first approximation to the effect.

Dilepton production via hadronic decay is limited, of course, to invariant masses for the pair at most equal to the mass of the parent hadron less any final state hadrons. Therefore, higher mass pairs can only come from very massive hadrons. One might even consider charmed non-strange and strange mesons, but even at these temperatures they would be rarely produced indeed. On the other hand, for intermediate dilepton invariant masses the results presented here lead naturally to questions about the role of axial vectors, the b_1 in particular, on the invariant mass spectrum of lepton pairs.

ACKNOWLEDGEMENT

This work was supported by the National Science Foundation under grant number PHY-9403666.

REFERENCES

- * electronic address: haglin@theo03.nsl.msui.edu
- [1] E. Shuryak, Phys. Rep. **67**, 71 (1980).
 - [2] E. L. Feinberg, Nuovo Cimento, A **34**, 39 (1976).
 - [3] E. V. Shuryak, Yad. Fiz. **28**, 796 (1978) [Sov. J. Nucl. Phys. **28**, 408 (1978)].
 - [4] K. Kajantie and H. I. Miettinen, Z. Phys. C **9**, 341 (1981).
 - [5] F. Halzen and H. C. Liu, Phys. Rev. D **25**, 1842 (1982).
 - [6] B. Sinha, Phys. Lett. **128B**, 91 (1983).
 - [7] R. C. Hwa and K. Kajantie, Phys. Rev. D **32**, 1109 (1985).
 - [8] G. Staadt, W. Greiner and J. Rafelski, Phys. Rev. D **33**, (1986).
 - [9] J. Kapusta, P. Lichard and D. Seibert, Phys. Rev. D **44**, 2774 (1991); Phys. Rev. D **47**, E4171 (1993).
 - [10] K. Haglin, C. Gale and V. Emel'yanov, Phys. Rev. D **47**, 973, (1993).
 - [11] L. Xiong, E. Shuryak and G. E. Brown, Phys. Rev. D **46**, 3798 (1992).
 - [12] C. Song, Phys. Rev. C **47**, 2861 (1993).
 - [13] K. Haglin and S. Pratt, Phys. Lett. B, in press.
 - [14] The $\rho(770)$ and $K^*(892)$ results are presented in [13], while the same approximations are used to calculate the numbers for $b_1(1235)$ and $K_1(1270)$.
 - [15] H. A. Weldon, Phys. Rev. D **28**, 2007 (1983).
 - [16] L. D. McLerran and T. Toimela, Phys. Rev. D **31**, 545 (1985).
 - [17] C. Gale and J. Kapusta, Nucl. Phys. **B357**, 65 (1991).
 - [18] U.-G. Meißner, Phys. Rep. **161**, 215 (1988).
 - [19] Particle Data Group, K. Hikasa *et al.*, Phys. Rev. D **45**, p. II.6–II.11 (1992).
 - [20] The formalism developed in [13] applied to $\pi\omega$ scattering through the b_1 gives a mean free path for ω of $\bar{\lambda}_\omega = 3.5, 1.2$ and 0.7 fermis at $T = 100, 150$ and 200 MeV, respectively.

FIGURES

FIG. 1. One-loop contribution to the photon self-energy including a_1 and K_1 axial-vector mesons (a) and two-loop contribution containing the ω —which further splits into a πb_1 loop in (b).

FIG. 2. Diagrams for radiative single-hadron decays $a_1 \rightarrow \pi\gamma$ and $K_1 \rightarrow K\gamma$ (a) and two-pion radiative decay of the b_1 in (b).

FIG. 3. Thermal photon production via axial-vector radiative decay at $T = 200$ MeV.

FIG. 4. Radiative decay of b_1 mesons at three temperatures 100, 150 and 200 MeV. The $b_1 \rightarrow \pi\pi^0\gamma$ results (solid curves) are compared with $\pi\rho \rightarrow \pi\gamma$ contributions (dashed curves) from Ref. [12].

FIG. 5. Collisional broadening of the ω through scattering with pions as a function of the ω momentum. Results for three temperatures are shown $T = 100, 150$ and 200 MeV.

FIG. 6. Comparison of $b_1 \rightarrow \pi\pi^0\gamma$ using the vacuum ω width (solid curves) and the rate using a collisional broadened width (dotted curves). Three temperatures are again shown, $T = 100, 150$ and 200 MeV.

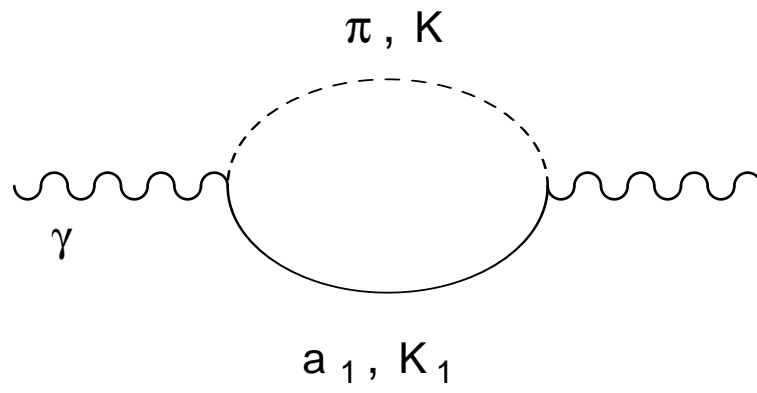
FIG. 7. Thermal production rate from the sum of three axial-vector radiative decays (solid curve) as compared with $\pi\rho \rightarrow \pi\gamma$ (dashed curve), $\pi\pi \rightarrow \rho\gamma$ (dotted curve) and $\rho \rightarrow \pi\pi\gamma$ (dot-dashed curve) at $T = 200$ MeV.

This figure "fig1-1.png" is available in "png" format from:

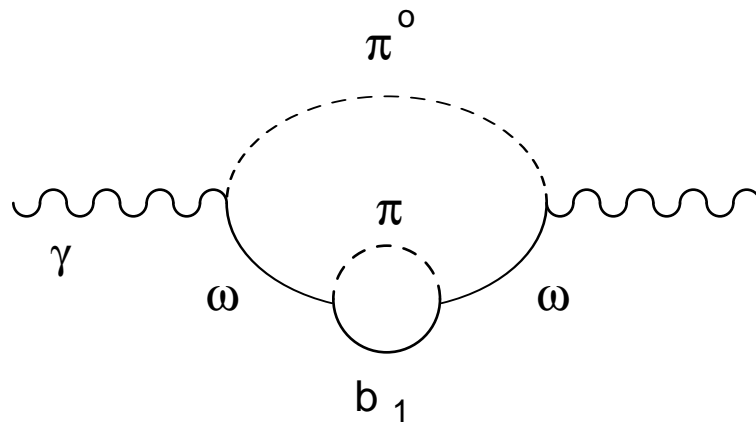
<http://arxiv.org/ps/nucl-th/9406026v1>

This figure "fig2-1.png" is available in "png" format from:

<http://arxiv.org/ps/nucl-th/9406026v1>



(a)



(b)

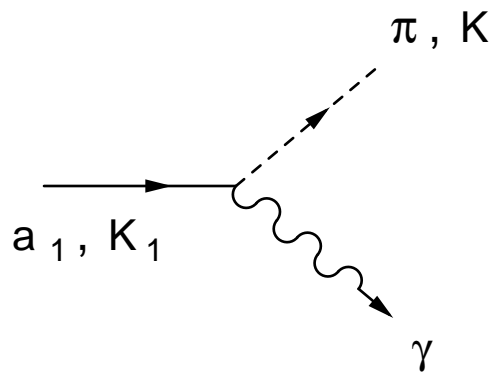
Figure 1

This figure "fig1-2.png" is available in "png" format from:

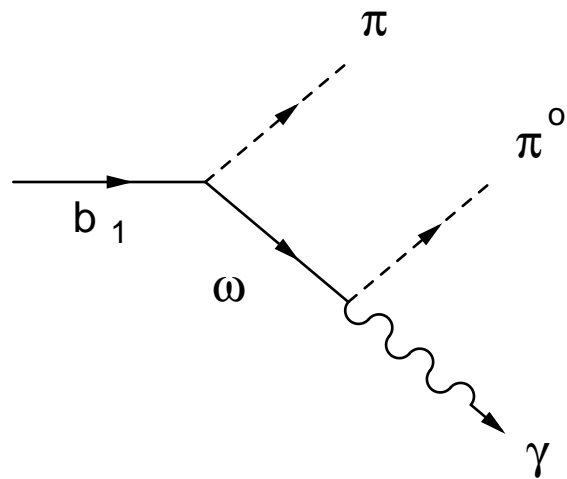
<http://arxiv.org/ps/nucl-th/9406026v1>

This figure "fig2-2.png" is available in "png" format from:

<http://arxiv.org/ps/nucl-th/9406026v1>



(a)



(b)

Figure 2

This figure "fig1-3.png" is available in "png" format from:

<http://arxiv.org/ps/nucl-th/9406026v1>

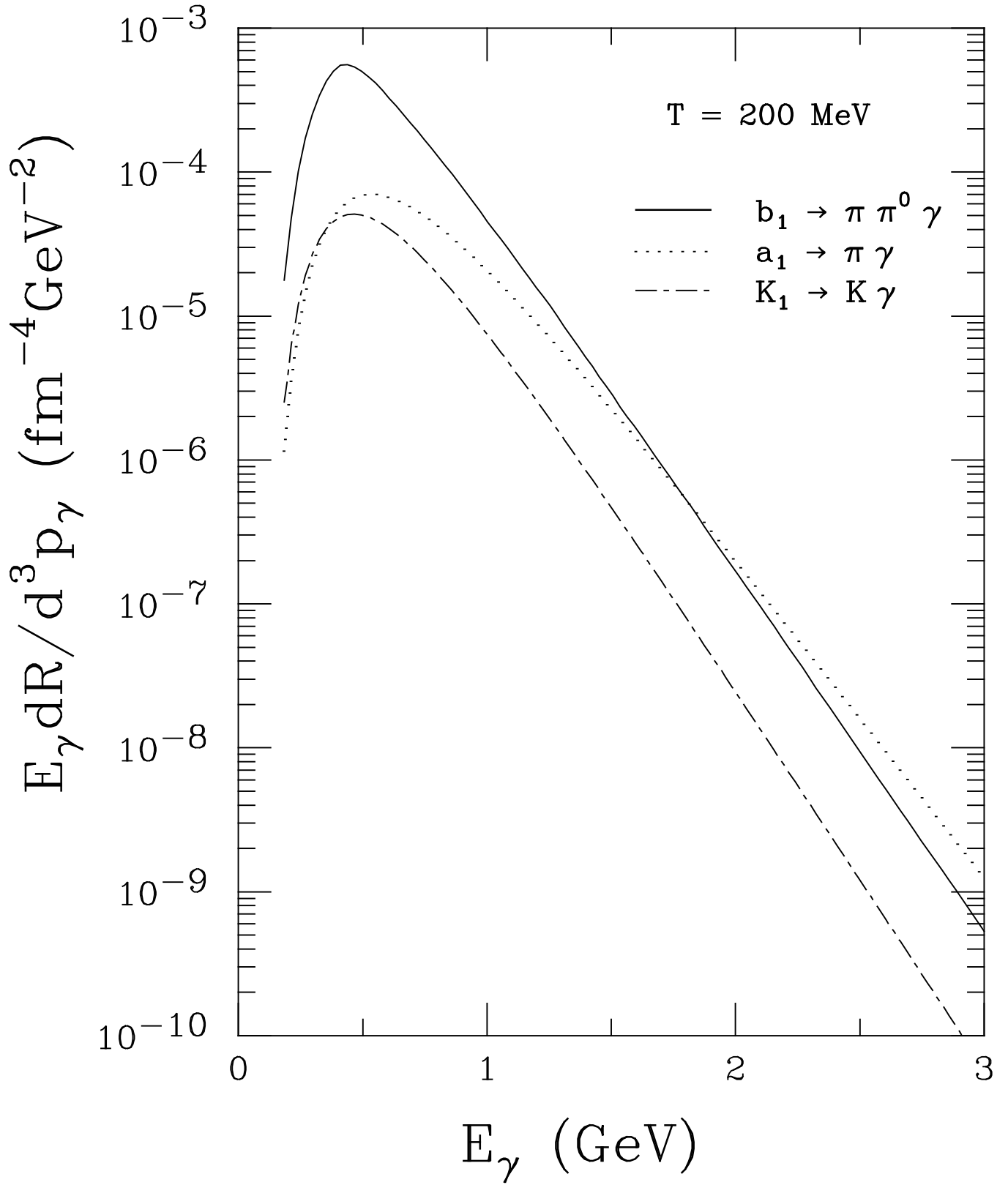


Figure 3

This figure "fig1-4.png" is available in "png" format from:

<http://arxiv.org/ps/nucl-th/9406026v1>

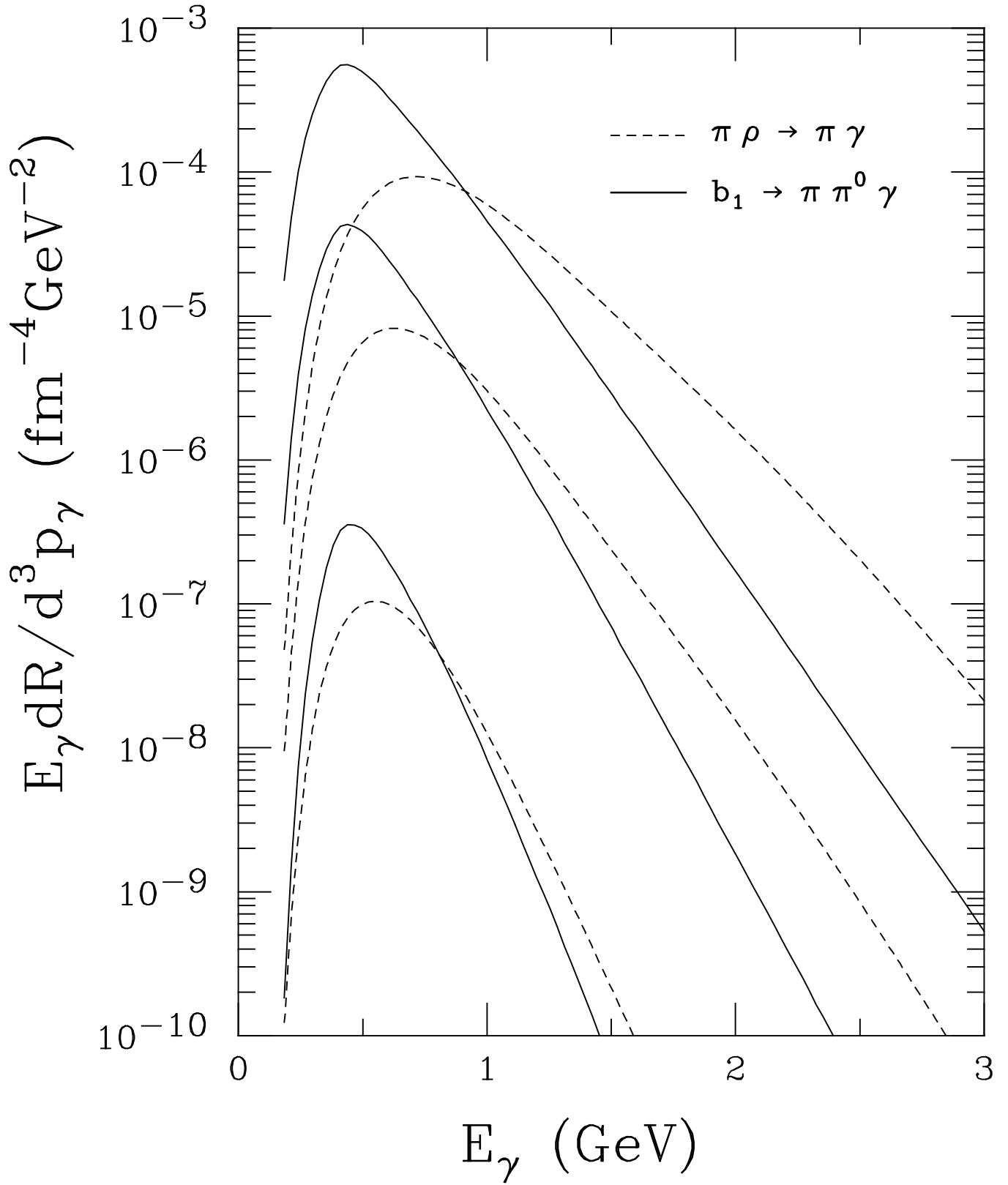
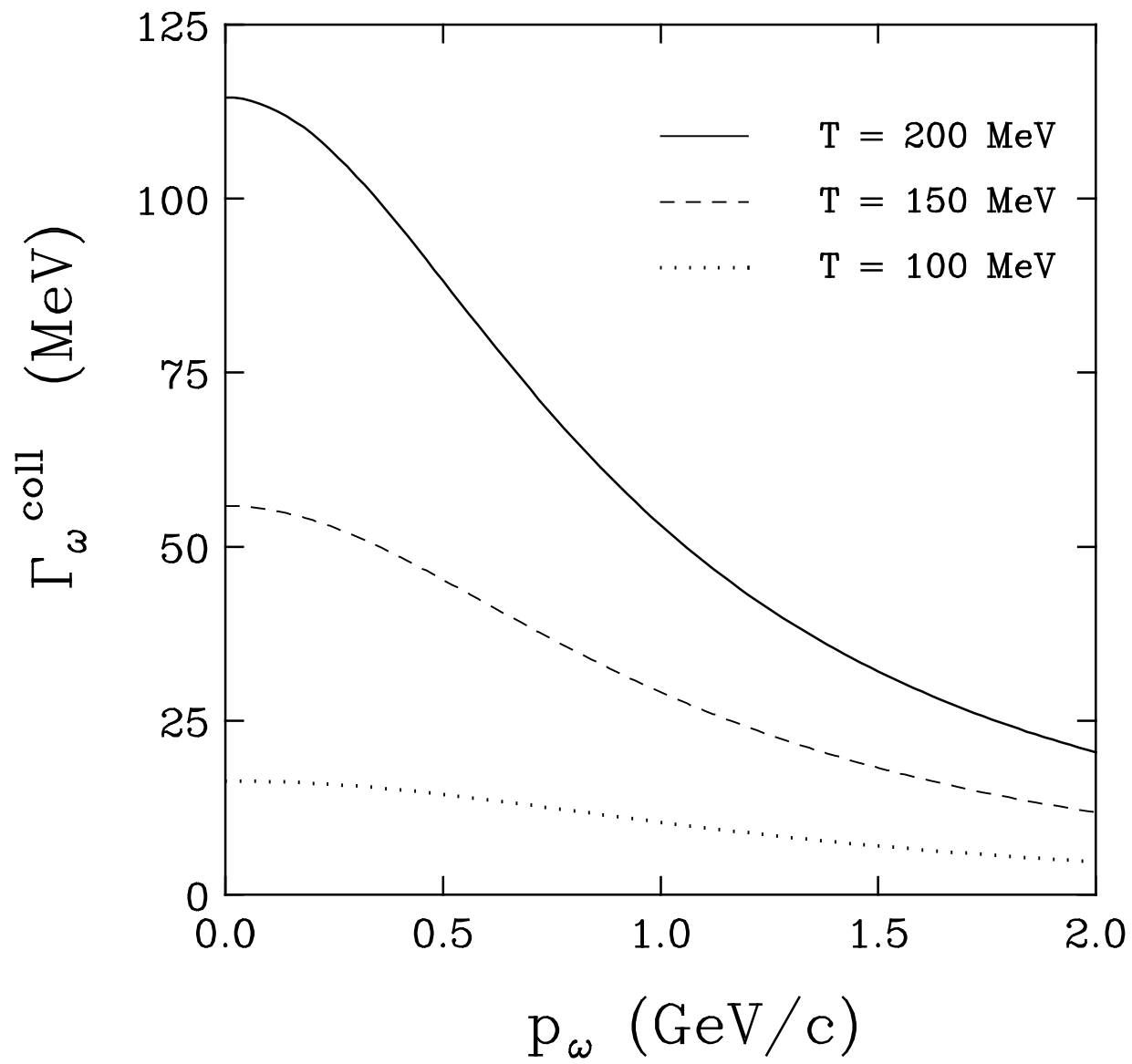


Figure 4

Figure 5



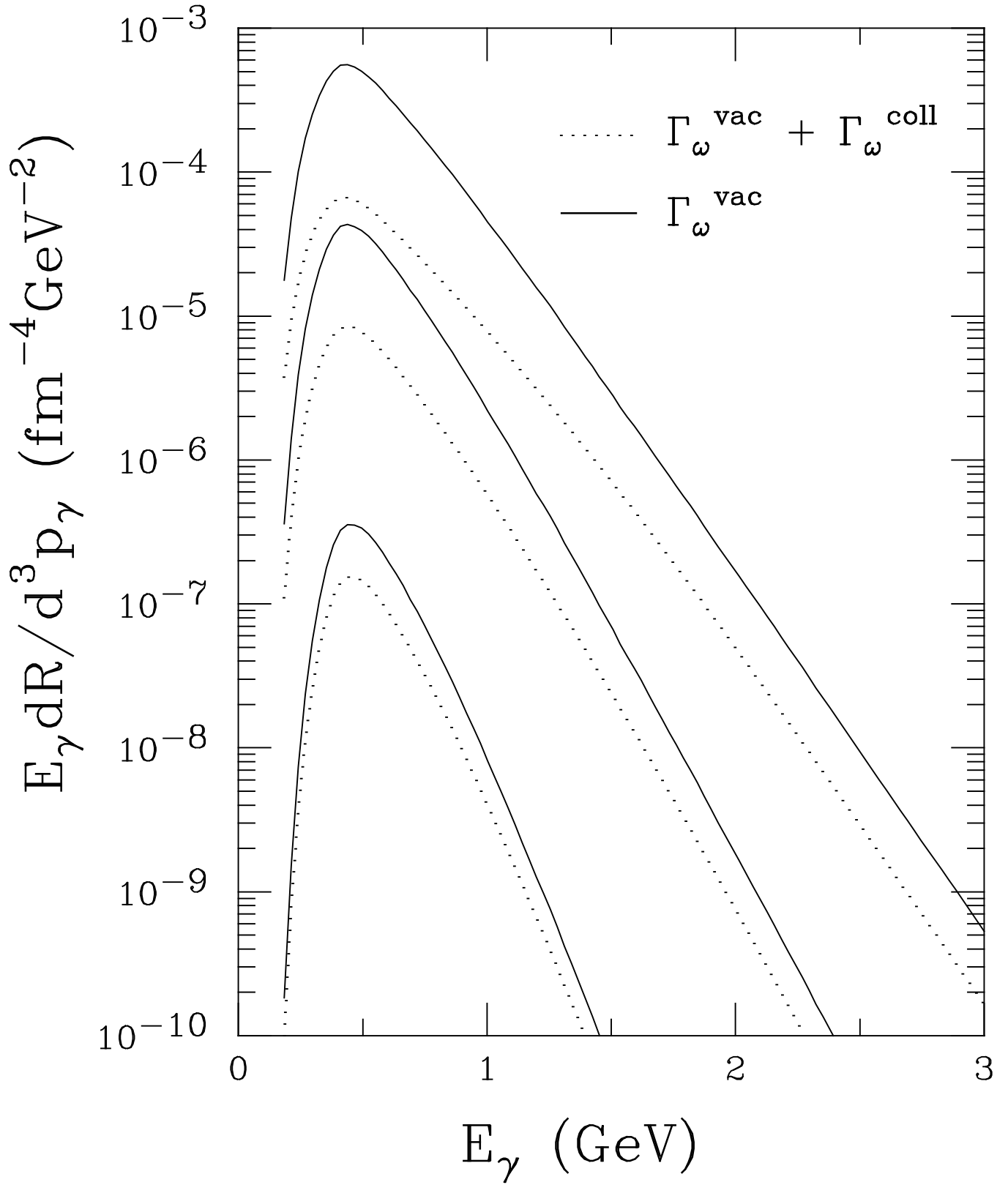


Figure 6

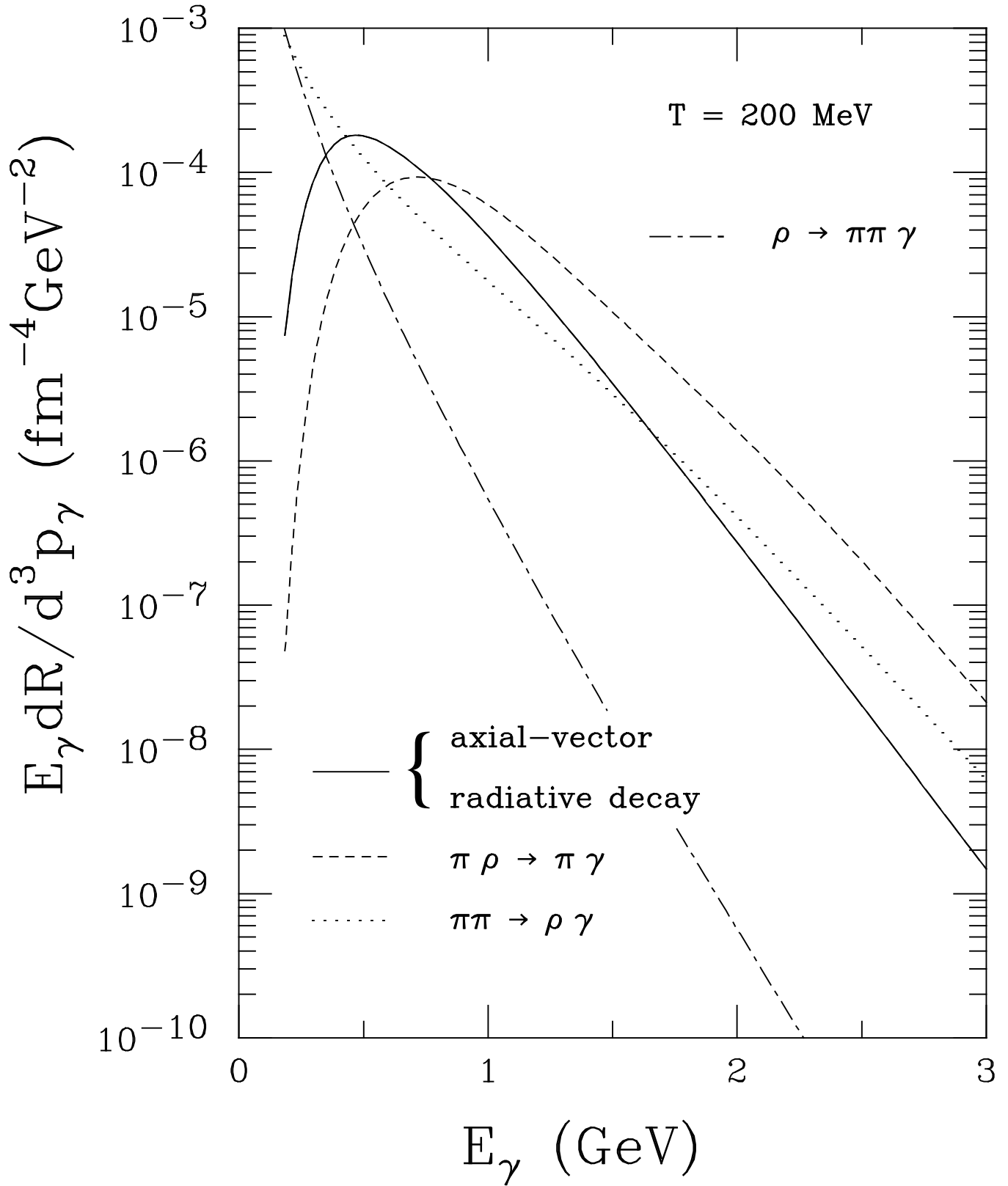


Figure 7